Tribological, Oxidation and Thermal Conductivity Studies of Microwave Synthesised Molybdenum Disulfide (MoS 2) Nanoparticles as Nano-Additives in Diesel Based Engine Oil

Thachnatharen Nagarajan
National Defence University of Malaysia
Mohammad Khalid (khalids@sunway.edu.my)
Sunway University
Nanthini Sridewi
National Defence University of Malaysia
Priyanka Jagadish
Sunway University
Syed Shahabuddin
Pandit Deendayal Petroleum University
Kasturi Muthoosamy
University of Nottingham Malaysia Campus (UMNC)
Rashmi Walvekar
Xiamen University Malaysia

Article

Keywords: MoS2, tribology, oxidative induction time (OIT), thermal conductivity, advanced microwave synthesis

Posted Date: April 15th, 2022

DOI: https://doi.org/10.21203/rs.3.rs-1552652/v1

Abstract

In this research, Molybdenum disulfide (MoS_2) nanoparticle was synthesised via microwave synthesis. Later, the nanoparticles were dispersed in SAE 20W50 diesel engine oil to formulate the nanolubricant. The results show that nanolubricant with 0.01 wt.% MoS_2 concentration showed the coefficient of friction (COF), average wear scar diameter (WSD) decreased by 19.24%, 19.52%, respectively, compared to the base oil. The nanolubricant with 0.01 wt.% concentration of MoS_2 nanoparticle showed the enhancement of 61.15% in Oxidation Induction Time (OIT) in comparison to the base oil. Furthermore, MoS_2 addition within the base oil demonstrates a ~ 10% improvement in thermal conductivity compared to the base oil.

Introduction

The automobile industry is well focused on emphasising eco-friendly, quality, durability, and energy efficiency properties. For example, 79% of the fuel is dissipated due to energy loss in a conventional passenger vehicle, as shown in Fig. 1 [1]. Energy loss and mechanical failure are caused mainly by friction and wear. Friction and wear consume around 1/3 of the global's predominant energy, and over half of the power accounts for the friction of transportation equipment [2]. Furthermore, worn-out parts account for almost 4/5 of mechanical failure [3]. Friction also contributes to significant issues such as surface corrosion and pollution of the environment. As a result, reducing friction and wear is critical for extending mechanical equipment service life, improving fuel efficiency, and lowering emissions.

Lubrication is one of the most reliable ways to reduce frictional wear, energy saving, environmental protection, and carbon decrement [4]. Many solutions have been used to reduce friction and wear to fulfil the objectives of conserving energy. Improving the groove texture profile under hydrodynamic lubrication conditions can increase the load-carrying capability of the oil film [5]. On the other hand, their tribological properties are commonly caused by frictional conditions, and they are prone to wear-out failure after a lengthy period of service. Since they may establish a hydrodynamic or elastohydrodynamic lubrication layer on the contact surface during frictional sliding, liquid lubricants are frequently used in the automotive industry [6]. In addition to lubricating oils, Ionic liquids can be used as liquid lubricants occasionally [7]. During the beginning and shutdown phases of mechanical parts, or when a high frictional environment occurs, liquid lubricants cannot establish a continuous lubricating layer in the middle of the frictional surfaces. In this context, boundary lubrication and mixed lubrication phases occur, resulting in increased friction and wear. The application of lubricant additives is the prominent method to decrease friction and wear by boundary lubrication [8]. Organic phosphates, organic sulphides, and organic metallic compounds are traditional lubricant additives with strong dispersion stability and tribological qualities. In terms of toxicology, the production of sulphated ash, phosphorous, and sulphur (SAPS), which can produce air contamination such as acid rain and hazy climate [9] and chemical erosion, are the issues that, environment face at varying degrees. Other additives, such as ionic liquids, have good tribological properties and are environmentally friendly, but they're pricey, limiting their application in the industry [10, 11]. Nanolubricants are described as the usage of nanoparticles as lubricant additives. Their particle diameter is usually in the range of 1 and 100 nm in diameter[12]. In situ experiments show that incorporating nanolubricants into base oils or coatings reduces friction and wear significantly while also exhibiting intriguing tribological properties. This study aims to improve the tribological qualities of diesel-based engine oil using nano-additives. This is the first attempt to synthesise MoS_2 nanoparticles using the microwave synthesis route for tribological application. The synthesis of nanoparticles using an advanced microwave synthesis method saves time, energy and produces better tribological, oxidation and thermal conductivity properties than the traditional hydrothermal method [13]. The physicochemical parameters of the MoS_2 nanoparticles were then determined, and the nanoparticles were dispersed in diesel-based engine oil to develop a novel nanolubricant. Following that, the tribological, oxidation, and thermal characteristics were investigated. The primary goal of this study is to create MoS_2 nanoparticles using advanced microwave technology, which have improved tribological, oxidation, and thermal properties when dispersed in diesel engine oil. This research will pave the path for developing new microwave-synthesised MoS_2 nano additives for diesel engine oil.

Results And Discussion

a) Characterisation of MoS_2 nanoparticle and nanolubricant

i. Field Emission Scanning Electron Microscope (FESEM) and Energy Dispersive X-Ray Spectroscopy (EDS) of MoS_2 nanoparticle.

Figure 2 shows the morphology of MoS_2 nanoparticles in (a) 50000x and (b) 100000x magnifications. The nanoparticles are equally distributed, well-faceted, multiple densely grown, semi-vertically and interleaving lamellar nanosheets with rough edges. These images confirmed the nanosheet morphology of the formed MoS_2. Figure 2 (b) displays the non-uniformed nanosheets with sizes approximately 150nm-300nm. However, several nanosheets are stacked up and seen agglomerated. The uniform and homogeneous distribution of molybdenum and sulfur across the nanosheet are shown in high-resolution EDS elemental mapping in Figures 2 (c) and (d). Figure 3 shows the sample's EDS spectrum of Mo (c) and S (d). Table 1 reveals the quantitative surface analysis of EDS carried out on the MoS_2 nanoparticles reveals the existence of sulfur and molybdenum in terms of atomic and weight percentage of constituents.

Table 1: The elemental distribution of MoS_2 nanoparticles

Element	Weight%	Atomic%
S	38.04	64.75
Mo	61.96	35.25
Totals	100.00	

ii. X-ray Diffraction (XRD) of MoS_2 nanoparticle

Figure 4 shows the XRD diffraction peaks of MoS_2 at 2 = 14.5°, 33.0°, 39.3°, 58.5°, and 69.7°, which can be referred to as the (002), (100), (103), (110), and (201) peaks of pure hexagonal MoS_2 phase according to JCPDS card no.371492, which are in accordance with previous studies [14, 15]. Peak broadening is seen, implying that the crystalline size is very small. For (100) and (103) XRD peaks, the magnitude dissimilarity between the reference pattern in the JCPD card and the synthesised nanoparticle is due to differences in texture of crystallite size difference and the size of the scattering domains. Other peaks of separate phases or impurities are not found in the XRD patterns, indicating that the crystal structure of MoS_2 nanosheets is in high purity form.

iii. Fourier-Transform Infrared Spectroscopy (FTIR) of MoS_2 nanoparticle.

Figure 5 displays the FT-IR spectra of the MoS_2 nanoparticle. The peaks were calculated or confirmed using the FTIR application library and the journals. Both samples have strong absorption bands at 485 cm^{-1}, 905 cm^{-1}, 1120 cm^{-1}, and 1665 cm^{-1}. The Mo-S bond is responsible for the band at 485 cm^{-1}, while the S-S bond is responsible for the band at 905 cm^{-1}. The stretching vibrations of the hydroxyl group and Mo-O vibrations are responsible for the absorption band between 1120 cm^{-1} and 1665 cm^{-1} [16]. By revealing the functional groups present in the study, the FT-IR spectra further confirm the formation of MoS_2.

iv. Visual Observation and Zeta Potential of MoS_2 nanolubricant

The stability of the MoS_2 nanolubricants against sedimentation via visual observation showed that the four various concentrations of 0.1wt. %, 0.05wt. %, 0.01wt. %, and 0.005wt. % of MoS_2 based nanolubricants were stable against sedimentation for 21 days (Figure 6). The zeta potential is significant as its magnitude is used to determine the stability of colloidal dispersions. As shown in Table 2, the zeta potential value of the MoS_2 nanolubricant with 0.05wt. %, 0.01wt. % and 0.005wt. % of MoS_2 concentrations is higher than 60 mV, indicating the nature of MoS_2 nanoparticle to be extremely stable in the nanolubricant. While 0.1wt. % shown lower zeta potential value, indicating poor stability in the engine oil as the nanoparticle concentration is the highest.

Dispersion with a higher zeta potential (negative or positive) is electrically stable, whereas those with a lower zeta potential agglomerate or flocculate. In general, the arbitrary value of 25 mV (positive or negative) distinguishes low-charged exterior from a highly charged exterior. Dispersion with a zeta potential of 40 to 60 mV is thought to be fairly consistent, whereas those with a zeta potential of more than 60 mV are considered to be extremely stable. The value of the zeta potential is directly proportional to the dispersion stability of the materials.

Table 2: Zeta potential magnitude of the MoS_2 nanolubricant with different concentrations

MoS_2 concentration in nanolubricant (wt. %)	Zeta potential (mV)
0.005	372.8
0.01	279.7
0.05	158
0.1	37

b) Tribological Analysis of MoS_2 nanolubricant

The coefficient of friction of MoS_2 nanolubricant with varying concentrations of MoS_2 nanoparticle wt. % in the base oil is shown in Figure 7. Without any nano-additives, the friction coefficient of the base oil was 0.0946. The friction coefficient of base oil with MoS_2 nanoparticles was found to be lower than pure base oil. In comparison to the base oil, the COF was reduced to 2%, 10.25 %, 19.24 %, and 11.73 % for 0.1wt. %, 0.05wt. %, 0.01wt. %, and 0.005wt. %, respectively. When the MoS_2 percentage in the nanolubricant was increased from 0.01wt. %, some MoS_2 nanoparticles agglomerate, resulting in larger secondary particle size. As a result, friction and wear would worsen, resulting in an increase in COF. The lowest concentration of MoS_2 nanoparticles, 0.005wt. % was insufficient to cover the entire contact surface, resulting in a greater COF than 0.01wt. % MoS_2. This suggests that 0.01 wt.% of MoS_2 nanolubricant is the best concentration for reducing COF. The sliding of nanosheets causes this phenomenon at asperities and deformed surfaces of individual nanosheets at interfaces to produce a protective layer known as the tribofilm, which decreases the COF[17-19]. The development of a tribofilm comprising nanosheets aids in reducing the friction caused by the individual layers of nanosheets slipping.

The findings show some damage caused by adhesive wear under the applied stress due to continuous sliding friction. Because of their higher surface energy and many dangling S bonds, MoS_2 nanoparticles can readily react and produce an abrasion-resistant protective coating at contacting surfaces. The MoS_2 nanosheets will be captivated into frictional surfaces, generating an adsorbed film and forming S-O or S-Fe bonds. The oxide layer on the substrate's surfaces provided the O and Fe. The adsorbed coating eliminated direct contact between frictional contacts and increased tribological characteristics [20]. The effect of firm boundary lubrication between the frictional pairs develops a protective tribofilm. Due to the adequate lubricity, this may result in an excellent ability to withstand shear failure.

Figure 8 presents wear scar diameter details of MoS_2 nanolubricant with various MoS_2 nanoparticle wt.% in base oil concentrations. The graphic of wear scar diameter created on the ball bearing during the tribological trials is depicted in figure 9. Without nanoparticles, the WSD for the base oil was 0.0953. When the ball bearing was tested for tribological aspects, the addition of MoS_2 nanoparticles in the base oil minimises the WSD. In comparison to the base oil, the WSD is reduced by 1.8 %, 10.6 %, 19.52 %, and 16.5 % for 0.1wt. %, 0.05wt. %, 0.01wt. %, and 0.005wt. %, respectively. The aforementioned information demonstrates that 0.01wt.% MoS_2 produces the best WSD in tribological analysis. Figure 9 shows that nanolubricant with higher concentrations of base oil (A), 0.1wt. % (B) and 0.05wt. % (C) exhibited darker concentric grooves, indicating abrasive wear, but smaller percentages of MoS_2, such as 0.01wt. % (D) and 0.005wt. % (E) exhibited smoother wear tracks, indicating decreases in the contact surfaces between the steel balls. The darker furrow is deeper, whereas the brighter furrow is shallower. Suresha et al. [21] made a similar observation. These ridges are responsible for depositing the MoS_2 nanoparticles firmly on the wear surface, which results in a reduction in wear. Huang et al. addressed a similar process with graphite sheets [22]. Hernandez et al. demonstrated that nanoparticles aggregate in the wear scar region in an experiment [23]. In comparison to the base oil containing MoS_2 nanoparticles, the wear scar image of the ball bearing lubricated by the base oil displayed many broad and deep ridges. The many MoS_2 nanosheets, we believe, penetrate more easily into the lubricant contact. Furthermore, nanosheets can create a continuous layer on rubbing surfaces because of their excellent adherence to contacts, improving tribological qualities. This phenomenon is known as the mending effect, where MoS_2 nanoparticles settle and occupy the grooves on the worn surface scratches of the rubbing surfaces, avoiding direct contact between the two surfaces and lowering the WSD. Those described above experimental tribological results imply that with an ideal concentration of 0.01wt% MoS_2 in the engine oil, both COF and WSD can be significantly improved.

According to the initial study, the formation of tribofilm and the mending effect is the fundamental mechanism for decreasing the frictional wear in the case of MoS_2 based nanolubricant. Due to the planar geometry of MoS_2, it may readily slide between the oil's surfaces. Furthermore, MoS_2 will cluster or agglomerate together and coagulate as the concentration increases, increasing wear and friction between surfaces. The segregation of interlayers into distinct layers is attributed to the wear process of MoS_2 nanosheets due to weaker van der Waals or Coulombic repulsive interactions at contact compulsion [24, 25]. These findings most likely indicate that adding MoS_2 to the lubricant significantly improves the nanolubricant's tribological capabilities.

c) Oxidation Analysis of MoS_2 nanolubricant

In the automobile industry, lubricants endure oxidation caused by intense temperature, high load, and air. Oxidation accelerates the degradation process of the base oils and additives, which decreases its performance, efficiency and life-span. The results of the OIT of the nanolubricants are shown in Figure 10. In comparison to the base oil, the OIT was improved by 12.17 %, 65.68 %, 61.15 % and 25.46% for 0.1wt. %, 0.05wt. %, 0.01wt. %, and 0.005wt. %, respectively. The nanolubricant with 0.05wt. % of MoS_2 nanoparticles showed the highest OIT compared with other concentrations of nanolubricant.

Due to the synergistic effect of MoS_2 with Zinc-dialkyl dithiophosphate (ZDDP), the nanolubricant's anti-oxidant characteristics were increased. The ZDDP additive is one of the most extensively employed additives in the automotive sector. It is most recognised for its antiwear characteristics, but it also contains anti-oxidant and extreme pressure characteristics. Phosphate glasses' capacity to digest oxides appears to be linked to ZDDP antiwear capabilities. Several authors [26-28] have demonstrated a synergistic interaction between MoDTC and ZDDP due to MoS_2 production. Lubricants undergo a three-step oxidation process. A free radical is produced at the first stage, initiation. The free radical combines with oxygen to produce peroxide radicals in the second stage called propagation. After combination with other lubricant components, these radicals have additional radicals. Two radicals join to form a stable molecule in the third phase, known as termination. The synergistic effect of MoS_2 with ZDDP promotes hydrogen donation, which stops the radical propagation process. It causes the nanolubricant's OIT to be higher. The nanolubricant with 0.1wt.%, 0.01wt.% and 0.005wt.% of MoS_2 nanoparticles possesses lower OIT than 0.05wt.% and 0.01wt.% as the mentioned concentration are not optimum in provide higher OIT in the nanolubricant. The substantial improvement in OIT of nanolubricants shows that the synergistic effect of MoS_2 nanoparticles and ZDDP can exhibit good oxidation stability, enhancing the antioxidant properties of the nanolubricants.

d) Thermal conductivity Analysis

From the tribological and oxidation analysis, the nanolubricant with 0.01wt. % MoS_2 nanoparticles provide the best result compared to other concentrations of MoS_2 nanoparticles in nanolubricant. Thus, it was further investigated for its thermal conductivity using the laser flash analysis method to compare the base oil. The addition of MoS_2 within the base oil demonstrates an improvement in thermal conductivity, as shown in figure 11. The thermal conductivity of the nanolubricant showed approximately~10 % of improvement as compared to the base oil. Due to the lower concentration of MoS2 nanoparticles (0.01wt. %), the noted improvement in thermal conductivity was caused bt the molecular collisions among the base oil and nanoparticles [29-33]. Moreover, perceived thermal conductivity behaviour during the investigation indicates that this enhancement is due to the percolation mechanism and the involvement of the Brownian motion of the nanosheet [34-36]. In addition, the nanoparticles' phonons get scattered in the active nanostructures, improving the contact conductance [37].

Subsequently, thermal conduction channels are developed, which improves thermal conductivity. This scenario is known as the percolation mechanism. In addition, the thermal transfer among the colliding nanoparticle rose the thermal conductivity of the nanolubricant. For example, from figure 11, the thermal conductivity of the nanolubricant rises more than the base oil after the temperature of 60 °C as a more intense Brownian motion of the nanoparticles occurs [38]. This thermal transport phenomenon in the nanolubricant was due to the physio-chemical attribute of the base oil, as well as collaboration with the reinforcement nanoparticles.

Conclusion

Nanolubricant with 0.01 wt.% MoS_2 shows the best results in reducing friction coefficient and wear scar diameter with 19.24% and 19.52% decrement compared to the COF of the base oil. Similarly, the nanolubricant containing 0.01 wt.% MoS_2 achieves excellent results with 61.15% enhancement in OIT compared to the base oil. Furthermore, when compared to the base oil, 0.01wt. % MoS_2 exhibits a ~ 10% improvement in thermal conductivity. Overall, the study shows 0.01 wt.% MoS_2 is suitable to enhance the lubricant performance.

Methods

a) Materials

All chemical substances utilised in the experiment were of analytical grade and used as received without further purification. Chemicals such as ammonium molybdate tetrahydrate ($(NH_4)6Mo_7O_{24}.4H_2O$) (Fisher Chemicals- Chicago, USA), thiourea ($SC(NH_2)_2$) (R&M Chemicals- Dundee, UK) and ethanol (CH_3CH_2OH) (Sigma-Aldrich, USA) were used for MoS_2 nanoparticle synthesis. The lubricant oil used was diesel engine oil with API SAE 20W50 CD/SE GL-4.

b) Preparation of MoS_2 nanoparticles using advanced microwave synthesis

To synthesise MoS_2 nanoparticles, all precursors were stoichiometrically measured and calculated as accurately as possible using a Sartorius PRACTUM224-1S analytical balance with a precision of ± 0.1 mg. Later, in 35 mL of deionised water, one mmol ammonium molybdate tetrahydrate ($(NH_4)6Mo_7O_{24}.4H_2O$) and 30 mmol thiourea ($SC(NH_2)_2$) were dissolved. The solution was stirred at 700 RPM for 20 min at room temperature with a Fisherbrand™ Isotemp™ hot plate stirrer. For synthesis reaction, a microwave platform system (Milestone flexiWAVE) was used. The homogeneous solution was transferred into a Teflon vessel of the microwave synthesis platform. The solution was heated to 200°C for 15 min. After the synthesis ended, the reaction mixture was left to cool naturally to room temperature (~26°C). The samples were then centrifuged using Sartorius Centrisart® D-16C (Göttingen, Germany) universal benchtop centrifuge with a maximum speed of 9,000 min^{-1}. The samples were washed several times with deionised water before being soaked in ethanol. The samples were then dried for 12 h in a Memmert UN55 gravity convection oven (Schwabach, Germany) at 70°C. The powder was then smoothly ground using a 50mm natural Agate mortar and pestle. Figure 12 illustrates the overall process involved in synthesising the MoS_2 nanoparticles.

c) MoS_2 based nanolubricant formulation

To synthesise the nanolubricant, 0.1wt. %, 0.05wt. %, 0.01wt. %, and 0.005wt. % of the collected MoS_2 nanoparticles were dispersed separately in 100ml of SAE 20W50 military-grade diesel engine oil. The mixture was then homogenised for 10 minutes at 5000 RPM using a Silverson L5M-A high shear lab mixer. The samples were sonicated further for 30 minutes in Cole-Parmer ultrasonic bath (Vernon Hills, USA) to enhance stability and ensure that all nanoparticles were uniformly mixed in the base oil without agglomeration. The formulated nanolubricants were highly stable for more than one week. Figure 13 depicts the overall process of nanolubricant formulation. The MoS_2 nanolubricants with various concentrations were prepared and stored in a sealed container under room temp for further analysis of their application, such as tribology, oxidation induction time and thermal conductivity.

d) Physio-chemical characterisation of MoS_2 nanoparticles and nanolubricant

MoS_2 nanoparticles were characterised physicochemically by Field Emission Scanning Electron Microscopy (FESEM), Energy-Dispersive X-ray spectroscopy (EDX), X-ray Diffractometer (XRD) and Fourier-Transform Infrared Spectroscopy (FTIR). In addition, MoS_2 nanolubricant were characterised by Zeta potential and visual observation. All physio-chemical characterisation of MoS_2 nanoparticles and nanolubricantas are as described follows:

i. Field Emission Scanning Electron Microscopy (FESEM) and Energy-Dispersive X-ray spectroscopy (EDX)

The size and morphology of MoS_2 nanoparticles were studied using an FEI Quanta 400F, USA, by attaching the samples on stubs with conductive carbon tape. The machine was run at a high vacuum of 20 kV. To obtain samples' morphological details, different magnifications from 50000x to 100000x were used. In addition, the elemental compositions of MoS_2 nanoparticles were also assessed using Energy-Dispersive X-ray spectroscopy (EDX).

ii. X-ray Diffractometer (XRD)

PANalytical X-ray Diffractometer was used to collect XRD data. A sample of MoS_2 nanoparticles was scanned from 20 to 80 degrees at a step size of 1 degree/min. The size of the divergence slit is 0.9570 degrees. Copper material was used to generate X-rays with a wavelength (K alpha) of 1.54 angstroms. X-rays were filtered through Ni using an operational voltage of 45 kV and a current of 27 mA.

iii. Fourier-Transform Infrared Spectroscopy (FTIR)

Fourier-Transform Infrared Spectroscopy (FTIR), Spectrum Two™ Perkin Elmer (L160000M), was employed to identify the functional groups of MoS_2 nanoparticles. The spectra were obtained from spectral wavenumber of 500 to 4000-1 with 200 scans.

iv. Zeta potential

The zeta potential of suspensions was determined using the Zetasizer Nano (Malvern, Worcestershire, UK) to determine their stability. Between the particle surface and the dispersion liquid, there is an electric potential at the sliding plane. The device combines electrophoresis and laser Doppler velocimetry, which

detects a particle's velocity in a liquid when electrical energy is exerted. Because the oil's viscosity index and dielectric constant are known, which is 115 and 2.4, the Henry equation uses the Smoluchowski equation to compute the Zeta potential.

v. Visual observation of nanolubricant

The stability of the MoS_2 nanolubricants against sedimentation was studied by visual observation. The samples in centrifuge tubes were visually monitored for stability against sedimentation for 21 days.

e) Evaluation of tribological properties of MoS_2 nanolubricant

A Ducom four-ball tribotester TR-30L was used to assess the COF and average WSD of MoS_2 nanolubricants with concentrations of 0.1wt. %, 0.05wt. %, 0.01wt. %, and 0.005wt. %, as well as the base oil. Steel balls were immersed in nanolubricants for tribological testing where a ball bearing rotates in contact with another three metal balls in a ball plot. The diameter of metal ball bearings that have utilised in the investigation was 12.7 mm. The physical parameters of the metal ball bearings used are listed in Table 3. In order to avoid contamination, the metal balls and associated apparatus were washed in ethanol and dried before tribological experiments. The rotational speed, applied load, time, and temperature were 12000 rpm, 392.5N, 3600 sec, and 75°C, according to the ASTM 4172-94 standard. Under the frictional contact of the four metal balls, the ASTM 4172-94 standard conditions aid in the early examination of the lubricant's antiwear qualities. Table 4 lists the operational parameters of a four-ball tribotester, while Fig. 14 illustrates the four-ball tribotester's experimental setup as well as a schematic depiction of the four-ball arrangement. The COF of the nanolubricant was determined by the main data processor on the tribotester. The diameter of the wear scar was evaluated by the image acquisition device. After the four-ball test, the worn scar diameter of the fixed metal balls is measured to ascertain the extent of wear. Throughout the experiment, the lubricant was maintained at a consistent temperature of 75°C. Following this, metal balls were washed with ethanol, and the worn scar was studied with an optical microscope. The coefficient of friction was measured by using Eq. (1)

$$\mu = 2.22707\frac{\tau}{p} \quad (1)$$

Where μ is the coefficient of friction for the experimental samples, the average frictional torque, τ in kg-cm and p, is the load exerted while carrying out the investigation.

Table 3
Physical properties of the metal ball-bearing

Properties	Ball-bearing
Material	Carbon-chromium steel
Hardness (*H*), HRC	1
Density (ρ), gm/cm3	7.79
Surface roughness (Ra),μm	0.022

Table 4
Operating Parameters for four-ball tribotester

Parameter	Purpose
Rotating speed	12000 rpm
Load applied	392.5N
Time	3600 sec
Temperature	75°C

f) Evaluation of the Oxidation Induction Time (OIT) properties of MoS_2 nanolubricant

The OIT of MoS_2 nanolubricants was determined using pressure-DSC at four various concentrations: 0.1wt. %, 0.05wt. %, 0.01wt. %, 0.005wt. %, and the base oil. These tests were achieved with the TA instrument's High-Pressure Differential Scanning Calorimeter (HP-DSC) 25P. The use of HP-DSC to study the oxidative stability of nanolubricants necessitates an airtight sample chamber. HP-DSC measures temperature flow for pressure-sensitive substances by attributing the heat flow of a blank reference pan to a sample pan. This procedure was carried out under accelerated conditions of 500 psi pressure and 200°C isothermal temperature. For all experiments, approximately 3.2mg of nanolubricant was placed into the HP-DSC, and the samples were first allowed to equilibrate at 50°C. Figure 15 represents a photograph of TA Instruments' High-Pressure Differential Scanning Calorimeter (HP-DSC) 25P, as well as a schematic drawing of the DSC's operation. Table 5 lists the operating parameters of the P-DSC. The relationship between the kinetic rate constant (k) and the temperature (T) in kinetic expressions, such as those governing OIT measurements, is given by the Arrhenius expression in (2)

$$k(T) = Z_{exp}^{\frac{-E}{RT}} \quad (2)$$

where:
k(T) is the specific rate constant at temperature T (1/min), Z represents the pre-exponential factor (1/min), E represents the activation energy (J/mol), R is the molar gas constant (8.3143 J/mol K), and T represents absolute temperature (K).

Table 5
Operating condition for P-DSC

Parameter	Purpose
Sample Amount	3 ± 0.3 mg
Gas	Ultra-high purity (UHP) grade oxygen
Flow rate	50 ml/min
Temperature	200°C
Pressure	500 psi
Ramp Rate	10°C /min

g) Evaluation of the thermal conductivity properties of MoS_2 nanolubricant

The samples were first injected into the sample ring with a syringe. The sample was then filled in the sample ring, which was critical for homogeneous irradiation. Finally, the upper and lower sealing discs were sprayed with graphite before assembling the sample holder's components to promote black body absorption. As shown in Fig. 16, the sample holder and samples were introduced into the NETZSCH 467 HT HyperFlash®. Figure 16 portrays an image of the instrument and a schematic diagram of the thermal conductivity analysis working principle. The heating was applied from room temperature to 140°C at a rate of 10°C/min. The chamber's atmosphere is nitrogen. The operating parameters of the NETZSCH 467 HT HyperFlash® are shown in Table 6.

Table 6
Operating condition for LFA

Parameter	Purpose
Gas	Ultra-high purity (UHP) grade Nitrogen
Heating rate	10°C/min
Temperature	Room temperature to 150°C

Declarations

Acknowledgement

The authors gratefully acknowledge Sunway University for awarding Individual Research Grant (GRTIN-IRG-03-2021). Also, the authors wish to thank the Research and Innovation Management Centre of the National Defence University of Malaysia for providing financial

Availability of Data and Materials

All data generated or analysed during this study are included in this published article. Additional data is available from the corresponding author on request.

References

1. Holmberg, K. and A. Erdemir, *The impact of tribology on energy use and CO_2 emission globally and in the combustion engine and electric cars*. Tribology International, 2019. **135**: p. 389–396.
2. He, F., G. Xie, and J. Luo, *Electrical bearing failures in electric vehicles*. Friction, 2020. **8**(1): p. 4–28.
3. Holmberg, K., et al., *Global energy consumption due to friction in trucks and buses*. Tribology International, 2014. **78**: p. 94–114.
4. Luo, J. and X. Zhou, *Superlubricitive engineering—Future industry nearly getting rid of wear and frictional energy consumption*. Friction, 2020. **8**: p. 643–665.
5. Wang, W., et al., *Optimization of groove texture profile to improve hydrodynamic lubrication performance: Theory and experiments*. Friction, 2020. **8**(1): p. 83–94.
6. Uzoma, P.C., et al., *Tribology of 2D Nanomaterials: A Review*. Coatings, 2020. **10**(9): p. 897.
7. Hua, J., et al., *Controllable friction of green ionic liquids via environmental humidity*. Advanced Engineering Materials, 2020. **22**(5): p. 1901253.

8. Deshpande, P., et al., *Effect of adding TiO 2 nanoparticles to a lubricant containing MoDTC on the tribological behavior of steel/steel contacts under boundary lubrication conditions*. Tribology Letters, 2020. **68**(1): p. 1–13.
9. Spikes, H., *Low-and zero-sulphated ash, phosphorus and sulphur antiwear additives for engine oils*. Lubrication science, 2008. **20**(2): p. 103–136.
10. Huang, G., et al., *Oil-soluble ionic liquids as antiwear and extreme pressure additives in poly-α-olefin for steel/steel contacts*. Friction, 2019. **7**(1): p. 18–31.
11. Jiang, C., et al., *Tribological evaluation of environmentally friendly ionic liquids derived from renewable biomaterials*. Friction, 2018. **6**(2): p. 208–218.
12. Shafi, W.K. and M. Charoo, *Nanolubrication systems: an overview*. Materials Today: Proceedings, 2018. **5**(9): p. 20621–20630.
13. Solomon, G., et al., *Microwave-Assisted vs. Conventional Hydrothermal Synthesis of MoS2 Nanosheets: Application towards Hydrogen Evolution Reaction*. Crystals, 2020. **10**(11): p. 1040.
14. Solomon, G., et al., *Ag2S/MoS2 nanocomposites anchored on reduced graphene oxide: fast interfacial charge transfer for hydrogen evolution reaction*. ACS applied materials & interfaces, 2019. **11**(25): p. 22380–22389.
15. Park, S.-K., et al., *A simple l-cysteine-assisted method for the growth of MoS 2 nanosheets on carbon nanotubes for high-performance lithium ion batteries*. Dalton Transactions, 2013. **42**(7): p. 2399–2405.
16. Nagaraju, G., et al., *Hydrothermal synthesis of amorphous MoS 2 nanofiber bundles via acidification of ammonium heptamolybdate tetrahydrate*. Nanoscale research letters, 2007. **2**(9): p. 461–468.
17. Ing, T.C., et al., *The effect of temperature on the tribological behavior of RBD palm stearin*. Tribology Transactions, 2012. **55**(5): p. 539–548.
18. Ordoñez, M., et al., *Tribofilm formation during dry sliding of graphite-and MoS2-based composites obtained by spark plasma sintering*. Tribology International, 2021: p. 107035.
19. Kohlhauser, B., et al., *Reactive in-situ formation and self-assembly of MoS2 nanoflakes in carbon tribofilms for low friction*. Materials & Design, 2021. **199**: p. 109427.
20. Xu, Y., et al., *Nano-MoS 2 and Graphene Additives in Oil for Tribological Applications*, in *Nanotechnology in Oil and Gas Industries*. 2018, Springer. p. 151–191.
21. Suresha, B., et al. *Tribological behaviour of pongamia oil as lubricant with and without halloysite nanotubes using four-ball tester*. in *AIP Conference Proceedings*. 2019. AIP Publishing LLC.
22. Huang, H., et al., *An investigation on tribological properties of graphite nanosheets as oil additive*. Wear, 2006. **261**(2): p. 140–144.
23. Battez, A.H., et al., *Wear prevention behaviour of nanoparticle suspension under extreme pressure conditions*. Wear, 2007. **263**(7–12): p. 1568–1574.
24. Fan, W., et al., *Vibrational spectrum renormalization by enforced coupling across the van der Waals gap between Mo S 2 and W S 2 monolayers*. Physical Review B, 2015. **92**(24): p. 241408.
25. Ma, H., Z. Shen, and S. Ben, *Understanding the exfoliation and dispersion of MoS2 nanosheets in pure water*. Journal of colloid and interface science, 2018. **517**: p. 204–212.
26. Grossiord, C., et al., *Tribochemical interactions between Zndtp, Modtc and calcium borate*. Tribology Letters, 2000. **8**(4): p. 203–212.
27. Muraki, M., Y. Yanagi, and K. Sakaguchi, *Synergistic effect on frictional characteristics under rolling-sliding conditions due to a combination of molybdenum dialkyldithiocarbamate and zinc dialkyldithiophosphate*. Tribology international, 1997. **30**(1): p. 69–75.
28. Bec, S., et al., *Synergistic effects of MoDTC and ZDTP on frictional behaviour of tribofilms at the nanometer scale*. Tribology Letters, 2004. **17**(4): p. 797–809.
29. Taha-Tijerina, J., et al. *2D structures-based energy management nanofluids*. in *ASME International Mechanical Engineering Congress and Exposition*. 2012. American Society of Mechanical Engineers.
30. Taha-Tijerina, J., et al., *Electrically insulating thermal nano-oils using 2D fillers*. Acs Nano, 2012. **6**(2): p. 1214–1220.
31. Ribeiro, H., et al., *Enhanced thermal conductivity and mechanical properties of hybrid MoS2/h-BN polyurethane nanocomposites*. Journal of Applied Polymer Science, 2018. **135**(30): p. 46560.
32. Zeng, Y.-X., et al., *Preparation and enhancement of thermal conductivity of heat transfer oil-based MoS2 nanofluids*. Journal of Nanomaterials, 2013. **2013**.
33. Yan, R., et al., *Thermal conductivity of monolayer molybdenum disulfide obtained from temperature-dependent Raman spectroscopy*. ACS nano, 2014. **8**(1): p. 986–993.
34. Lee, S., et al., *Molecular dynamic simulation: Studying the effects of Brownian motion and induced micro-convection in nanofluids*. Numerical Heat Transfer, Part A: Applications, 2016. **69**(6): p. 643–658.
35. Peña-Parás, L., et al., *Temperature dependence of the extreme-pressure behavior of CuO and TiO2 nanoparticle additives in metal-forming polymeric lubricants*. Industrial Lubrication and Tribology, 2017.
36. Teruel, M., et al., *2D MoSe2-based nanofluids prepared by liquid phase exfoliation for heat transfer applications in concentrating solar power*. Solar Energy Materials and Solar Cells, 2019. **200**: p. 109972.
37. Shin, S. and R. Chen, *Thermal transport measurements of nanostructures using suspended micro-devices*. Nanoscale Energy Transp, 2020: p. 12–1.
38. Ribeiro, H.I., et al., *Hybrid MoS2/h-BN nanofillers as synergic heat dissipation and reinforcement additives in epoxy nanocomposites*. ACS applied materials & interfaces, 2017. **11**(27): p. 24485–24492.

Figures

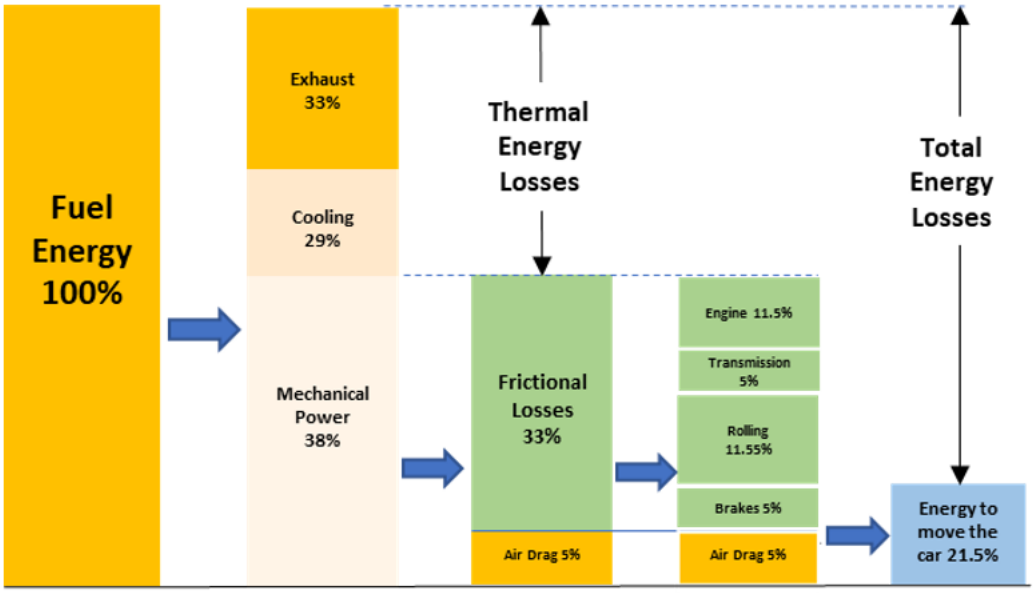

Figure 1

Energy consumption breakdown for passenger cars [1]

Figure 2

(a) and (b) Field Emission Scanning Electron Microscope (FESEM) (c) and (d) Energy Dispersive X-Ray Spectroscopy (EDS) mapping of the synthesised MoS_2 nanoparticle

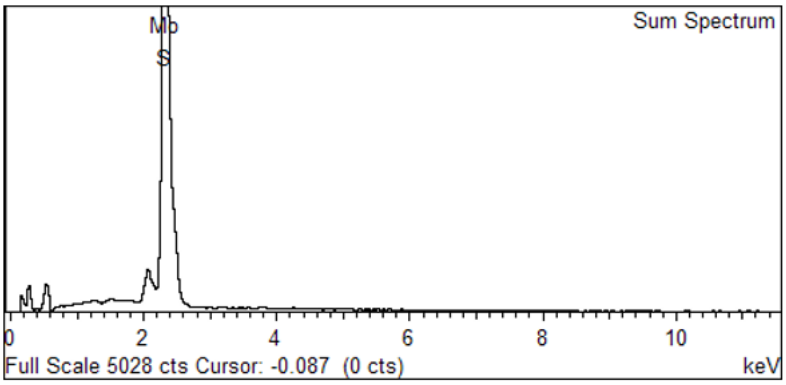

Figure 3

The EDS Spectrum of the MoS_2 nanoparticles

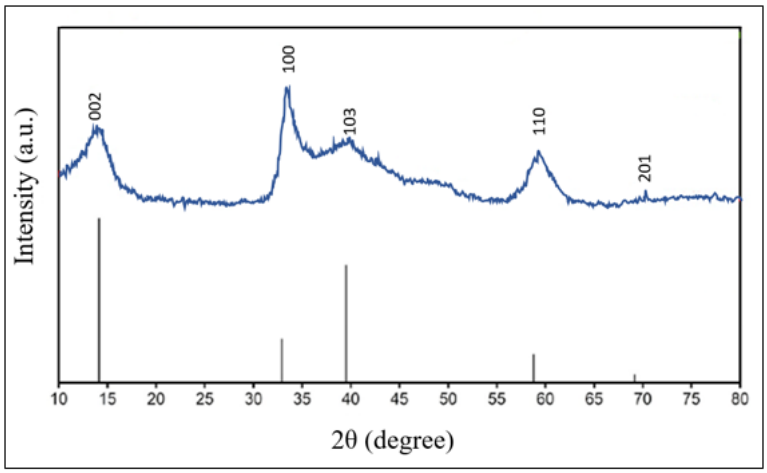

Figure 4

XRD pattern of MoS_2 nanoparticles

Figure 5

FTIR spectroscopy graph of MoS_2 nanoparticle

Figure 6

Visual observation of the dispersion stability of MoS_2 nanolubricants at varying concentrations

Figure 7

COF of MoS_2 nanolubricant

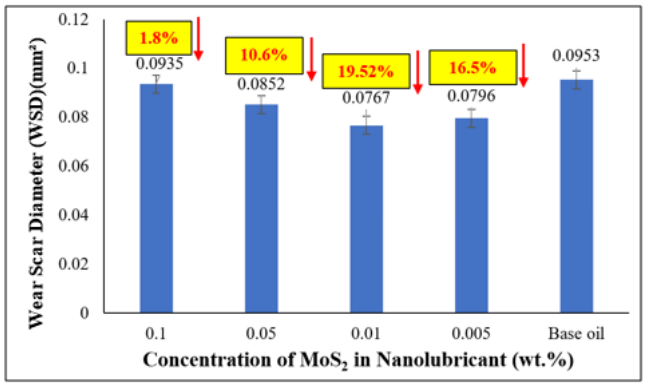

Figure 8

Average WSD profile on MoS_2 nanolubricant

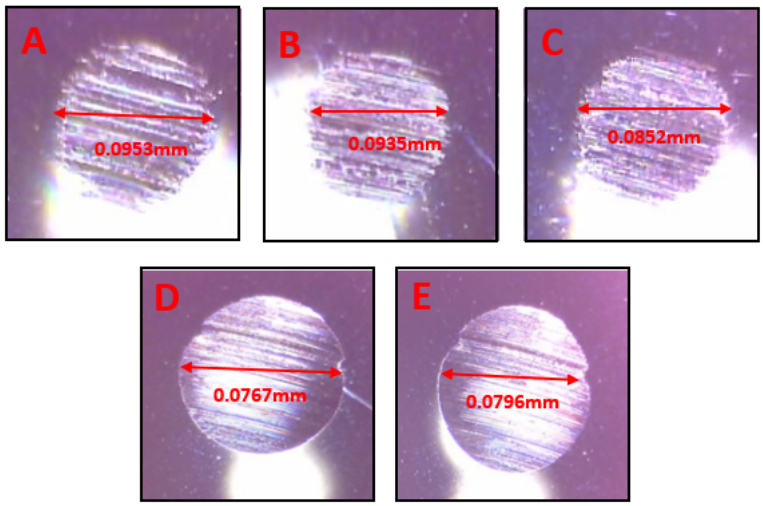

Figure 9

Ball bearing image after tribological experiments using MoS_2 nanolubricant

Figure 10

OIT of MoS_2 nanolubricant with different concentrations

Figure 11

Thermal conductivity of 0.01wt. % nanolubricant with base oil.

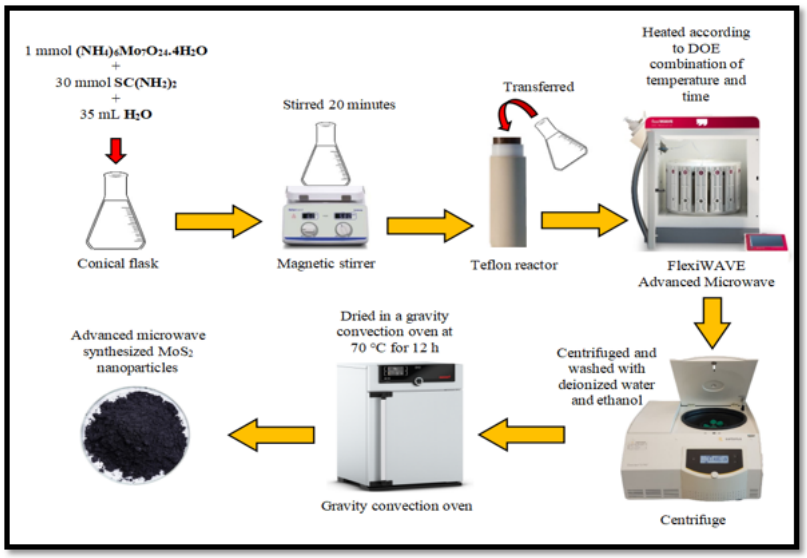

Figure 12

Schematic diagram of MoS_2 nanoparticles preparation via advanced microwave synthesis

Figure 13

Process flow of MoS_2 nanolubricant formulation

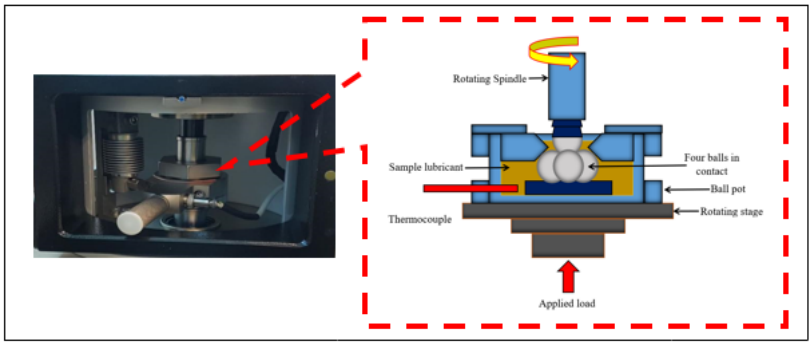

Figure 14

The experimental setup and the schematic drawing of the tribotester

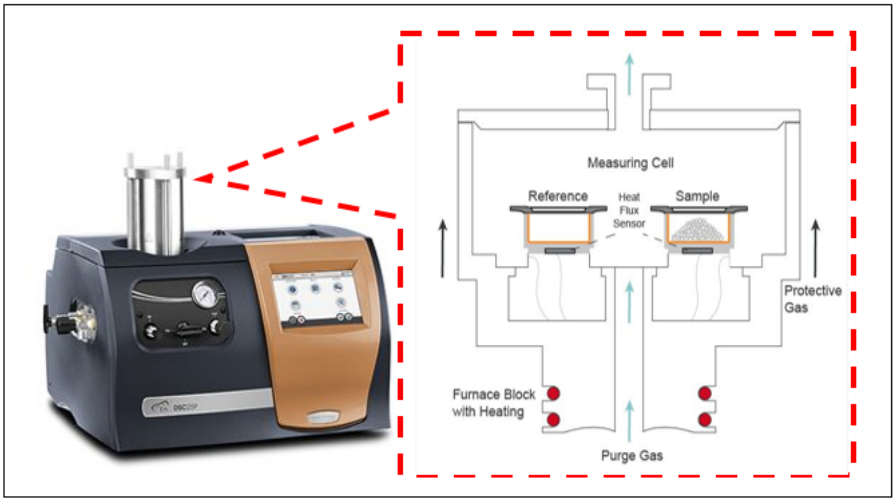

Figure 15

HP-DSC and the schematic drawing of the HP-DSC working principle

Figure 16

LFA and the schematic drawing of the LFA working principle